Effect of body deformability on microswimming

Journal Name

ARTICLE TYPE

Cite this: DOI: 10.1039/xxxxxxxxxx

Effect of body deformability on microswimming†

Jayant Pande,[a,b] Laura Merchant,[a,b,c‡] Timm Krüger,[d] Jens Harting,[e,f] and Ana-Sunčana Smith*[a,b,g]

Received Date
Accepted Date

DOI: 10.1039/xxxxxxxxxx

www.rsc.org/journalname

In this work we consider the following question: given a mechanical microswimming mechanism, does increased deformability of the swimmer body hinder or promote the motility of the swimmer? To answer this we run immersed-boundary-lattice-Boltzmann simulations of a microswimmer composed of deformable beads connected with springs. We find that the same deformations in the beads can result in different effects on the swimming velocity, namely an enhancement or a reduction, depending on the other parameters. To understand this we determine analytically the velocity of the swimmer, starting from the forces driving the motion and assuming that the deformations in the beads are known as functions of time and are much smaller than the beads themselves. We find that to the lowest order, only the driving frequency mode of the surface deformations contributes to the swimming velocity, and comparison to the simulations shows that both the velocity-promoting and velocity-hindering effects of bead deformability are reproduced correctly by the theory in the limit of small bead deformations. For the case of active deformations we show that there are critical values of the spring constant–which for a general swimmer corresponds to its main elastic degree of freedom–which decide whether the body deformability is beneficial for motion or not.

1 Introduction

The study of microswimmer motion has gained a lot of impetus recently, driven in equal measure by advances in experimental technology,[1–12] numerical methods,[13–17] and theoretical modelling.[18–24] The increased attention has served to highlight the dazzling variety of ways in which nature accomplishes the difficult task of achieving non-reversibility of motion, as is required for propagation at low Reynolds numbers,[25] although only a few degrees of freedom are available to micro-organisms compared to their macro-scale cousins.

In spite of their great diversity, a large number of microswimmers can be classified as mechanical, as their motion is driven by different parts of their body moving in coordinated yet asymmetric ways, leading to a corresponding asymmetry in the fluid flow surrounding them and thereby motion. In nature, this class of microswimmers is predominant.[26–30] For artificial swimmers, chemically driven mechanisms are as popular as mechanical ones.[31–37]

An important consideration in mechanical microswimming is the way elastic forces interact with the fluid and any external forces present in determining the motion. In the literature different aspects of these forces that have been studied are the elasticity of swimming appendages,[14,38] the influence of flexible surrounding walls if the motion occurs close to them,[39,40] and even the elasticity (or the viscoelasticity) of the ambient fluid.[8,41–49] In addition, the advantage of having elastic bodies has been investigated for the forced motion of micro-bodies, such as capsules driven through constrictions.[50]

While the role of deformable swimming appendages (like cilia and flagella for biological swimmers,[14,38] and harmonic springs for artifical models[51,52]) has been well-studied in the literature, one facet of elasticity that has so far not been adequately considered is the consequence of having a passively deformable *swimmer body*. When a swimmer has an elastic, yielding body, it under-

[a] *PULS Group, Department of Physics, Friedrich-Alexander-University Erlangen-Nuremberg, Nägelsbachstraße 49b, 91054 Erlangen, Germany.*
[b] *Cluster of Excellence: Engineering of Advanced Materials, Friedrich-Alexander-University Erlangen-Nuremberg, Nägelsbachstraße 49b, 91054 Erlangen, Germany.*
[c] *School of Physics and Astronomy, University of St. Andrews, North Haugh, St. Andrews KY16 9SS, The United Kingdom.*
[d] *School of Engineering, The University of Edinburgh, Edinburgh EH9 3JL, The United Kingdom.*
[e] *Helmholtz Institute Erlangen-Nuremberg for Renewable Energy (IEK-11), Forschungszentrum Jülich, Fürther Straße 248, 90429 Nuremberg, Germany.*
[f] *Department of Applied Physics, Eindhoven University of Technology, P.O. Box 513, 5600MB Eindhoven, The Netherlands.*
[g] *Division of Physical Chemistry, Ruđer Bošković Institute, Bijenička cesta 54, 10000 Zagreb, Croatia. Fax: +49 9131 85 20860; Tel: +49 9131 85 20842; E-mail: smith@physik.fau.de*

† Electronic Supplementary Information (ESI) available: *Mathematica* notebook showing the velocity of a swimmer with deformable beads and allied expressions. See DOI: 10.1039/b000000x/

‡ Presently at the University of Glasgow.

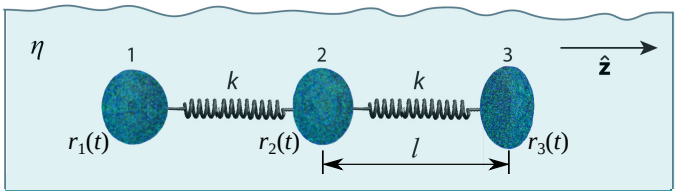

Fig. 1 (Colour online) A swimmer composed of three deformable closed membranes connected by springs.

goes deformations of body shape in response to the fluid pressure that it faces. These deformations, which we term *passive* in contrast to *active* shape deformations which occur under the swimmer's own agency,[21,53,54] modify continuously both the friction coefficient of the swimmer and the fluid flow around it. Small changes in swimmer morphology, whether actively or passively induced, can have a big influence on the swimming behaviour, as is illustrated by some bacteria for which size changes of 0.1 μm can cause a 100000 times higher energetic cost of motion.[55]

In the literature, the only existing theoretical consideration of the role of passive body deformations on microswimming is by Ohta and collaborators, who study an active, deforming Brownian particle moving with an assumed velocity in the undeformed state.[56–66] In contrast with their approach of positing a coupling between the swimming velocity and the body deformations, in this article we present a fully-resolved description of the motion of a swimmer as a result of all the forces acting upon it, and the differences that emerge when the swimmer body becomes deformable.

Our model of study is a swimmer composed of deformable beads connected in a line through springs and driven by sinusoidal forces (Fig. 1; explained in detail in the next section), an extension of the three-sphere swimmer introduced by Najafi and Golestanian.[67] The latter swimmer is a popular one in the field owing to its simplicity, and as we show in this paper, our extension of it retains this simplicity while imparting to it the features that are needed to investigate the influence of body deformations on microswimming.

We perform fully-resolved immersed-boundary-lattice-Boltzmann simulations of the swimmer, modelling the beads through membranes with a number of stiffness moduli which specify their responses to different deformation forces. Unlike many other realisations of swimmers based on spheres changing their relative distances,[13,20,21] the stroke of the swimmer is not imposed in our simulations but emerges in response to the forces driving the system. In addition, the surfaces of the beads undergo passive deformations due to the fluid pressure they face. Our simulations are the first in our knowledge wherein the response of a microswimmer, with elasticity both in the swimming body and swimming appendages, to the forces acting on it is fully resolved in 3D.

The simulations show that the same deformations in the beads can result in both a rise and a fall in the swimming velocity, depending on the various system parameters. With the help of an analytical model which takes the bead surface deformations to be given, we find the precise way in which the interplay between the bead deformations and the other parameters affects the swimming velocity. Finally, for *active* deformations wherein all the beads deform identically, we show that it is the spring stiffness which decides whether the deformability of the beads is beneficial to the swimming or not.

2 Swimmer simulations

Our microswimmer is made up of three deformable beads which are closed membranes with an incompressible Newtonian fluid inside which is identical to the external fluid in which the swimmer is placed (Fig. 1). For performing simulations with this model we employ the LB3D code,[68,69] which combines the lattice-Boltzmann method (LBM)[70] for the fluid, the finite element method (FEM) for the membrane deformations, and the immersed boundary method (IBM)[71] for the coupling between the fluid and the membranes. The lattice structure employed in our simulations is the D3Q19 lattice and the collision operator is given by the Bhatnagar-Gross-Krook (BGK) model, both standard choices.

The different possible deformations that the beads undergo are strain, bending and changes in volume and surface area. The energy of deformation W_i of the i^{th} bead is given by

$$W_i = W_i^{\mathrm{S}} + W_i^{\mathrm{B}} + W_i^{\mathrm{V}}, \tag{1}$$

where the superscripts S, B and V label the energy contributions due to strain, bending and volume change, respectively. Expressions for all these energy contributions are listed in Appendix A1. Note that in our simulations the global surface area of the beads is allowed to change freely.

The three beads in the swimmer are initially spherical with initial radii $r_i = 5\Delta x$ $(i = 1,2,3)$, where Δx denotes one lattice cell length. The beads are aligned collinearly along the z-axis with harmonic springs connecting them (Fig. 1). For simplicity, we take the springs to have equal rest lengths $l = 36\Delta x$ and equal stiffness constants $k = 0.02\rho(\Delta x)^3/(\Delta t)^2$, where ρ denotes the density of the fluid (both internal and external) and Δt is one time step. The fluid dynamic viscosity is $\eta = 0.2\rho(\Delta x)^2/\Delta t$.

The beads are driven by known forces which sum to zero at all times, in order to model autonomous swimming. These forces act on the centres of the beads and are assumed to be of the form

$$\begin{aligned} \mathbf{F}_1^{\mathrm{d}}(t) &= A\sin(\omega t)\,\hat{\mathbf{z}}, \\ \mathbf{F}_2^{\mathrm{d}}(t) &= -\mathbf{F}_1^{\mathrm{d}}(t) - \mathbf{F}_3^{\mathrm{d}}(t), \text{ and} \\ \mathbf{F}_3^{\mathrm{d}}(t) &= B\sin(\omega t + \alpha)\,\hat{\mathbf{z}}, \text{ with } \alpha \in [-\pi, \pi]. \end{aligned} \tag{2}$$

A and B specify the amplitudes of the driving forces $\mathbf{F}_1^{\mathrm{d}}(t)$ and $\mathbf{F}_3^{\mathrm{d}}(t)$ which are applied to the leftmost and the rightmost beads, respectively, and α denotes the phase difference between them. A, B and α vary in the different simulations. The driving frequency for all the simulations is $\omega = 2\pi/(8000\Delta t)$.

The deformable bead membranes are modelled by meshes which have 720 triangular faces each, and are generated by successively subdividing an initially coarse icosahedron mesh. As the beads deform, we constrain their volume deviations to be

Table 1 Parameters for two simulations of the swimmer with some beads deformable. The parameters which are common to all the simulations, namely r, l, ω, k_i^{V}, k_i^{B}, k and η, are stated in section 2. The shear moduli k_i^{S} (equal to the local area moduli k_i^{α}) are given in units of $\rho(\Delta x)^2/(\Delta t)^2$. Here $\mathbf{v}_{\mathrm{relative}} = (\mathbf{v}_{\mathrm{def}} - \mathbf{v}_{\mathrm{rigid}})/|\mathbf{v}_{\mathrm{def}}|$.

	k_1^{S}	k_2^{S}	k_3^{S}	A/B	α	$\mathbf{v}_{\mathrm{relative}}$
(a)	0.1	0.1	0.1	20	$\pi/2$	$-0.067\ \hat{\mathbf{z}}$
(b)	1.0	0.1	0.1	1	0	$1.0\ \hat{\mathbf{z}}$

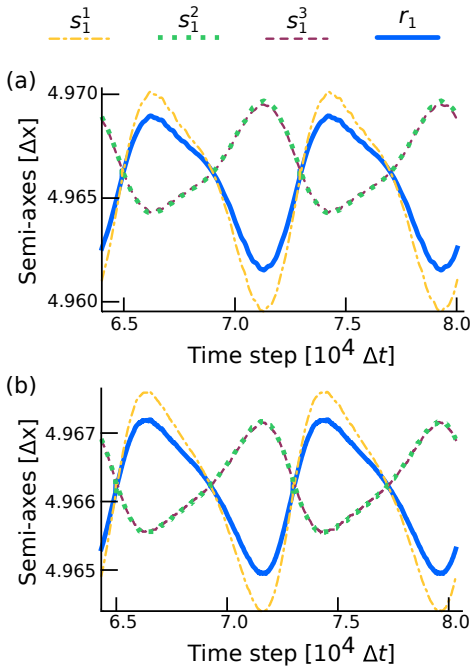

Fig. 2 (Colour online) The three semi-axes s_1^1, s_1^2 and s_1^3 of the bounding ellipsoid of bead 1, and the resultant effective radius r_1, over two swimming cycles, in two simulations with parameters stated in Table 1.

smaller than 0.01% by setting the volume change modulus to $k_i^{\mathrm{V}} = 1.0\rho(\Delta x)^2/(\Delta t)^2$. The bending modulus is kept fixed, at a value of $k_i^{\mathrm{B}} = 10^{-3}\rho(\Delta x)^5/(\Delta t)^2$, since varying it by 5 orders of magnitude changes the swimming velocity by less than 1% (data not shown), due to the initially spherical shape of the beads. In order to reduce the parameter space, the shear moduli k_i^{S} and the local area moduli k_i^{α} are changed together in the simulations, *i.e.* always such that $k_i^{\mathrm{S}} = k_i^{\alpha}\ \forall\ i$. Physically this means that the membranes respond equally strongly to both shear and dilation.

3 Effect of bead deformability

To study the effect of surface deformability of the beads in the above model on the motility, we compare the velocities of swimmers with rigid beads (denoted as $\mathbf{v}_{\mathrm{rigid}}$) and with deformable beads (denoted as $\mathbf{v}_{\mathrm{def}}$), as found from the LB3D simulations.

We find that, in general, bead deformability can both enhance and hinder the swimming velocity. In fact, in all our simulations, if we fix all the other parameters in the problem and only change the bead deformabilities, then the velocity either monotonically increases or monotonically decreases with the bead deformability.

To understand why this happens, we examine the deformations of the bead surfaces that are generated in the simulations. For this we quantify the shape deformations through the instantaneous 'effective hydrodynamic radius' $r_i(t)$ of the i^{th} bead, defined via the drag force on the bead as

$$r_i(t) = \frac{\gamma_i(t)}{6\pi\eta}, \tag{3}$$

where $\gamma_i(t)$ is the Stokes drag coefficient of the bead. The effective hydrodynamic radius is sometimes also called the 'reduced friction coefficient' of a body immersed in a fluid in Stokes flow.

Since the surface deformations in our simulations are not too large and the beads retain a convex shape throughout, we approximate the instantaneous shape of a bead by an ellipsoid of the same inertia tensor.[72] Due to the axisymmetry in our simulations, at each moment two of the semi-axes of such an ellipsoid are equal, although the ellipsoid can change from prolate to oblate and back within a swimming cycle. The effective hydrodynamic radius $r_i(t)$ of the bead at each instant is then calculated as the reduced friction coefficient of the corresponding ellipsoid, using Perrin's formulas.[51,73]

Surprisingly, we find that the surface deformations of swimmers whose velocity is enhanced by the deformability, and those whose velocity is hindered, are very similar. As an illustration, Fig. 2 plots the three semi-axes s_1^1, s_1^2 and s_1^3 and the resulting effective hydrodynamic radius $r_1(t)$ of bead 1 in two simulations whose parameters are detailed in Table 1. Despite the bead deformations in the two simulations being qualitatively close to indistinguishable, we find that the swimmer in Table 1(a) becomes slower when all its beads are made rigid (demonstrated by the negative sign of $\mathbf{v}_{\mathrm{relative}} = (\mathbf{v}_{\mathrm{def}} - \mathbf{v}_{\mathrm{rigid}})/|\mathbf{v}_{\mathrm{def}}|$), while the one in Table 1(b) becomes faster. This means that it is not the surface deformations themselves which determine whether the velocity increases or decreases upon making the swimmer body more deformable, but some other property in the swimmer.

4 Analytical velocity calculation

Since the surface deformations alone do not help us distinguish between the cases of velocity increase and decrease, we now assume them to be of a given form and aim to find how their interplay with the other parameters of the swimmer affects its velocity. In particular, we first find the $r_i(t)$ functions from the simulations as described in section 3, and then analytically determine the velocity of the swimmer, for this purpose extending our method for swimmers with rigid beads.[51,74] This approach decouples the fluid flow and the bead surface deformations by implicitly supposing that the latter are weak enough to not affect the flow directly. Such a condition is recovered in the limit of small bead deformations and large bead separations, and we will show that in this limit our approach correctly predicts an increase or decrease in the swimming velocity with the bead deformability.

We assume that all motion occurs in the Stokesian regime, so that the fluid flow is governed by the equations

$$\eta\nabla^2\mathbf{u}(\mathbf{r},t) - \nabla p(\mathbf{r},t) + \mathbf{f}(\mathbf{r},t) = \mathbf{0}, \text{ and} \tag{4}$$

$$\nabla\cdot\mathbf{u} = 0, \tag{5}$$

where $\mathbf{u}(\mathbf{r},t)$ and $p(\mathbf{r},t)$ are the velocity and the pressure, respectively, of the fluid at the point $\mathbf{r}$ at time t. The force density $\mathbf{f}(\mathbf{r},t)$ acting on the fluid is given by

$$\mathbf{f}(\mathbf{r},t) = \sum_{i=1}^{3} \left(\mathbf{F}_i^{\mathrm{d}}(t) + \mathbf{F}_i^{\mathrm{s}}(t) \right) \delta\left(\mathbf{r} - \mathbf{R}_i(t)\right), \tag{6}$$

where the index $i = 1,2,3$ denotes the i-th bead placed at the position $\mathbf{R}_i(t)$ subject to a driving force $\mathbf{F}_i^{\mathrm{d}}(t)$ and a net spring force $\mathbf{F}_i^{\mathrm{s}}(t)$. The latter can be written as

$$\mathbf{F}_i^{\mathrm{s}}(t) = \sum_{j \neq i} \mathbf{G}\left(\mathbf{R}_i(t) - \mathbf{R}_j(t)\right), \text{ with}$$

$$\mathbf{G}\left(\mathbf{R}_i(t) - \mathbf{R}_j(t)\right) = -k \left(\frac{\mathbf{R}_i(t) - \mathbf{R}_j(t)}{|\mathbf{R}_i(t) - \mathbf{R}_j(t)|} \right) \left(|\mathbf{R}_i(t) - \mathbf{R}_j(t)| - l \right) \tag{7}$$

if i and j denote neighbouring beads, and $\mathbf{G}\left(\mathbf{R}_i(t) - \mathbf{R}_j(t)\right) = \mathbf{0}$ otherwise. Assuming no slip at the fluid-bead interfaces, the instantaneous velocity $\mathbf{v}_i(t)$ of each bead is given by[75]

$$\mathbf{v}_i(t) = \dot{\mathbf{R}}_i(t) = \left(\mathbf{F}_i^{\mathrm{d}}(t) + \mathbf{F}_i^{\mathrm{s}}(t) \right) / \left(6\pi\eta r_i(t)\right) + \sum_{j \neq i}^{3} \mathbf{T}\left(\mathbf{R}_i(t) - \mathbf{R}_j(t)\right) \cdot \left(\mathbf{F}_i^{\mathrm{d}}(t) + \mathbf{F}_i^{\mathrm{s}}(t) \right), \tag{8}$$

where $\mathbf{T}(\mathbf{r})$ is the Oseen tensor[76,77] and $r_i(t)$, as before, is the instantaneous effective hydrodynamic radius of the i^{th} bead. Here in $\dot{\mathbf{R}}_i(t)$ and throughout the paper, a dot over a variable denotes its derivative with respect to time.

In the simulations it is seen that the swimmer, like its rigid bead counterpart,[74] swims in the steady state with a constant cycle-averaged velocity with the individual beads oscillating around this uniformly-moving configuration. Consequently, the positions of the centres of the beads in the steady state can be written in the form

$$\mathbf{R}_i(t) = \mathbf{S}_{i0} + \xi_i(t) + \mathbf{v}_{\mathrm{def}} t, \tag{9}$$

where $\xi_i(t)$ denotes small sinusoidal oscillations, which will be taken as perturbation variables around the equilibrium configuration $\mathbf{S}_{i0}$ of the swimmer which moves with the uniform cycle-averaged velocity $\mathbf{v}_{\mathrm{def}}$. Note that in Eq. (9), $\mathbf{S}_{i0}$ are known functions defined by the initial (unperturbed) configuration while $\xi_i(t)$ and $\mathbf{v}_{\mathrm{def}}$ need to be determined.

For our calculation we need to know the bead effective hydrodynamic radii $r_i(t)$ as functions of time, and we determine these from the simulations as explained in section 3. In general, given any periodic form for $r_i(t)$, it can be expressed in a Fourier series in ωt of the form

$$r_i(t) = a_i + \sum_{n=1}^{\infty} b_i^n \sin\left(n\omega t + \phi_i^n\right), \quad i = 1,2,3, \tag{10}$$

where a_i is the mean radius of the i^{th} bead, and b_i^n and ϕ_i^n are the amplitude and the phase shift, respectively, of the contribution from the n^{th} frequency mode. We consider only small bead deformations (a restriction which allows us to ignore the back reaction onto the fluid flow from the deforming surfaces) subject to the conditions

$$b_i^n / a_j \ll 1 \quad \text{and} \quad b_i^n / |\xi_j(t)| \ll 1 \tag{11}$$

for all i, j, and n and time t. Note that since the dominant length in the problem is the mean distance l between the beads, the above conditions set in a further separation of the length scales, with $b_i^n \ll a_j \ll l$ and $b_i^n \ll |\xi_j(t)| \ll l \;\forall\; i, j, n$ and t.

In Stokes flow, the position of the whole assembly is defined by that of the centre of reaction $\mathbf{C}(t)$, which takes the place of the centre of mass in other settings and is given by[76]

$$\mathbf{C}(t) = \frac{\sum_{i=1}^{3} r_i(t)\mathbf{R}_i(t)}{\sum_{i=1}^{3} r_i(t)}. \tag{12}$$

Since the changes in $r_i(t)$ are assumed to be small, the time-dependence in $\mathbf{C}(t)$ arises mainly from $\mathbf{R}_i(t)$, and the cycle-averaged swimming velocity $\mathbf{v}_{\mathrm{def}}$ can then be written as

$$\mathbf{v}_{\mathrm{def}} = \frac{\omega}{2\pi} \int_0^{2\pi/\omega} \mathrm{d}t \dot{\mathbf{C}}(t) = \frac{\omega}{2\pi} \int_0^{2\pi/\omega} \mathrm{d}t \frac{\sum_{i=1}^{3} r_i(t)\dot{\mathbf{R}}_i(t)}{\sum_{i=1}^{3} r_i(t)}. \tag{13}$$

Expanding $\dot{\mathbf{C}}(t)$ from Eqs. (10) and (13), we have

$$\dot{\mathbf{C}}(t) = \frac{\sum_{i=0} \left(a_i + \sum_{n=1}^{\infty} b_i^n \sin\left(n\omega t + \phi_i^n\right) \dot{\mathbf{R}}_i(t) \right)}{\left(\sum_{j=1}^{3} a_j \right) \left(1 + \sum_{k=1}^{3} \sum_{m=1}^{\infty} \bar{b}_k^m \sin(m\omega t + \phi_k^m) \right)}, \tag{14}$$

where $\bar{b}_k^m = b_k^m / \sum_{l=1}^{3} a_l$. Here $\dot{\mathbf{R}}_i(t)$ can be written, using Eqs. (7)-(10), as

$$\dot{\mathbf{R}}_i(t) = \frac{\mathbf{F}_i^{\mathrm{d}}(t) + \sum_{j \neq i}^{3} \mathbf{G}\left(\mathbf{R}_i(t) - \mathbf{R}_j(t)\right)}{6\pi\eta \left(a_i + \sum_{n=1}^{\infty} b_i^n \sin\left(n\omega t + \phi_i^n\right) \right)} + \sum_{j \neq i}^{3} \mathbf{T}\left(\mathbf{R}_i(t) - \mathbf{R}_j(t)\right) \cdot \left(\mathbf{F}_j^{\mathrm{d}}(t) + \sum_{k \neq j}^{3} \mathbf{G}\left(\mathbf{R}_i(t) - \mathbf{R}_j(t)\right) \right). \tag{15}$$

Following the method of Felderhof,[78] we expand the functions of $\left(\mathbf{R}_i(t) - \mathbf{R}_j(t)\right)$ above in terms of series of the variables $\left(\xi_i(t) - \xi_j(t)\right)$ centred around the equilibrium configuration, which can be taken to be the configuration at time $t = 0$. The different variables expanded to the first order in $\left(\xi_i(t) - \xi_j(t)\right)$

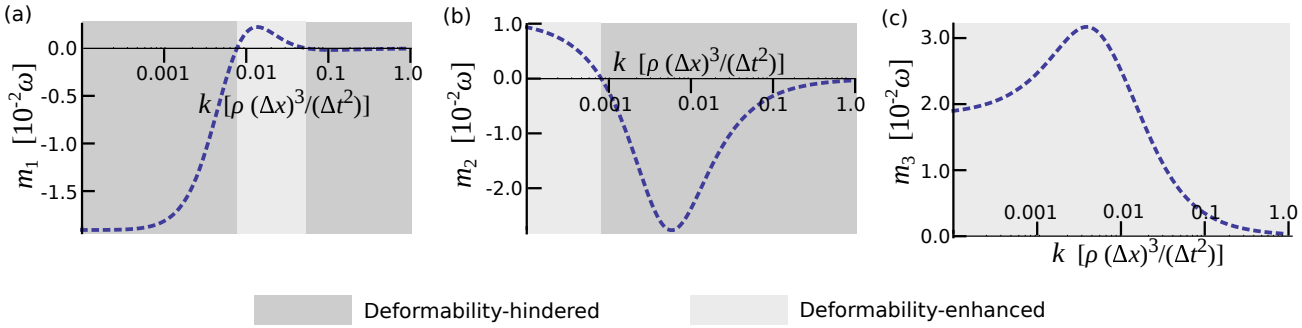

Fig. 3 (Colour online) The coefficients m_i ($i = 1,2,3$), which determine the dependence of the swimming velocity on the bead deformability $b_i^1(t)$, as functions of the spring constant k. For the i^{th} individual bead, the deformability-enhanced and -hindered regions are defined as those where m_i is respectively larger and smaller than 0.

are

$$\mathbf{G}\left(\mathbf{R}_i(t)-\mathbf{R}_j(t)\right) =$$

$$\mathbf{G}\left(\mathbf{R}_i(0)-\mathbf{R}_j(0)\right) + \left.\frac{\partial \mathbf{G}\left(\mathbf{R}_i(t)-\mathbf{R}_j(t)\right)}{\partial \mathbf{R}_i(t)}\right|_{t=0} \cdot \left(\xi_i(t)-\xi_j(t)\right)$$

$$= \mathbf{H}_{ij}\cdot\left(\xi_i(t)-\xi_j(t)\right), \text{ with } \mathbf{H}_{ij} = \left.\frac{\partial \mathbf{G}\left(\mathbf{R}_i(t)-\mathbf{R}_j(t)\right)}{\partial \mathbf{R}_i(t)}\right|_{t=0}, \quad (16)$$

and

$$\mathbf{T}\left(\mathbf{R}_i(t)-\mathbf{R}_j(t)\right) =$$

$$\mathbf{T}\left(\mathbf{R}_i(0)-\mathbf{R}_j(0)\right) + \left.\frac{\partial \mathbf{T}\left(\mathbf{R}_i(t)-\mathbf{R}_j(t)\right)}{\partial \mathbf{R}_i(t)}\right|_{t=0} \cdot \left(\xi_i(t)-\xi_j(t)\right)$$

$$= \mathbf{T}_{ij} + \mathbf{V}_{ij}\cdot\left(\xi_i(t)-\xi_j(t)\right), \quad (17)$$

$$\text{with } \mathbf{T}_{ij} = \mathbf{T}\left(\mathbf{R}_i(0)-\mathbf{R}_j(0)\right) \text{ and } \mathbf{V}_{ij} = \left.\frac{\partial \mathbf{G}\left(\mathbf{R}_i(t)-\mathbf{R}_j(t)\right)}{\partial \mathbf{R}_i(t)}\right|_{t=0}. \quad (18)$$

Combining Eqs. (14)-(17) and using the fact that $\mathbf{F}_i^{\text{d}}(t)$ and $\mathbf{F}_i^{\text{s}}(t)$ always sum to zero over the three bodies , we get

$$\dot{\mathbf{C}}(t) = \frac{\left(1-\sum_{p=1}^{3}\sum_{m=1}^{\infty}\bar{b}_p^m \sin(m\omega t+\phi_p^m)\right)}{\sum_{j=1}^{3} a_j} \times$$

$$\sum_{i=1}^{3}\sum_{j\neq i}^{3}\left\{\left(a_i+\sum_{n=1}^{\infty} b_j^n \sin(n\omega t+\phi_j^n)\right)\cdot\left(\mathbf{T}_{ij}+\left(\xi_i(t)-\xi_j(t)\right)\cdot\mathbf{V}_{ij}\right)\cdot \left(\mathbf{F}_j^{\text{d}}(t)+\sum_{k\neq j}^{3}\left(\xi_j(t)-\xi_k(t)\right)\mathbf{H}_{jk}\right)\right\}. \quad (19)$$

Making use of the condition $b_i^n/|\xi_j(t)| \ll 1$, we expand all terms in Eq. (13) to the lowest surviving order in $\xi_i(t)$ after inserting in it the expression for $\dot{\mathbf{C}}(t)$ from Eq. (19). Since the displacements $\xi_i(t)$ directly arise from the driving forces $\mathbf{F}_j^{\text{d}}(t)$, this also means the lowest surviving order in $\mathbf{F}_j^{\text{d}}(t)$.[78] Moreover, since both the displacements and the driving forces are sinusoidal, it turns out that all terms in Eq. (13) of the zeroth or first order in $\xi_i(t)$ or $\mathbf{F}_j^{\text{d}}(t)$ average to zero over a cycle. Checking now for the second order terms, it is found that only the $n = 1$ terms for the surface fluctuation $\sum_{n=1}^{\infty} b_i^n \sin(n\omega t+\phi_i^n)$ contribute, since all the other modes also evaluate to zero due to the orthogonality of the sinusoidal functions.

Therefore, given sufficiently weak periodic surface deformations of any functional form, only the driving frequency modes contribute to the swimming motion. The terms that survive in Eq. (19) are all sinusoidal functions, and the equation then becomes straightforward to solve, finally yielding an expression for $\mathbf{v}_{\text{def}}$ of the form

$$\mathbf{v}_{\text{def}} = \mathbf{v}_{\text{rigid}} + \sum_{i=1}^{3} m_i b_i^1 \hat{\mathbf{z}}. \quad (20)$$

Here $\mathbf{v}_{\text{rigid}}$ is the velocity of a corresponding swimmer with all beads rigid (see Appendix A2 for an analytical expression for the same), and the coefficients m_i (Fig. 3), which have the units of frequency, are independent of the shape deformation amplitudes b_j^1. Due to their length, the expressions for the m_i's are provided in the Electronic Supplementary Information ESI in the form of a *Mathematica* file.

5 Comparison between theory and simulations

Eq. (20) helps explain why similar bead deformations can result in qualitatively different effects on the swimming velocity (as seen from Fig. 2 and Table 1). Whether the deformations of the i^{th} bead cause the velocity to rise or drop depends on the sign of m_i, and the three m_i's are functions of the fluid viscosity, the driving forces, the springs, the radii of the beads and the phase shifts between their deformations (see the ESI). Since the m_i's are independent of the deformations b_i^1's themselves, the velocity is always a monotonic function of b_i^1.

Fig. 3 plots the m_i's as functions of the spring constant k with the other parameters held constant. The light (dark) grey regions in the three parts of the figure mark the values of k for which the surface deformations of each individual bead increase (decrease) the swimming velocity. We label

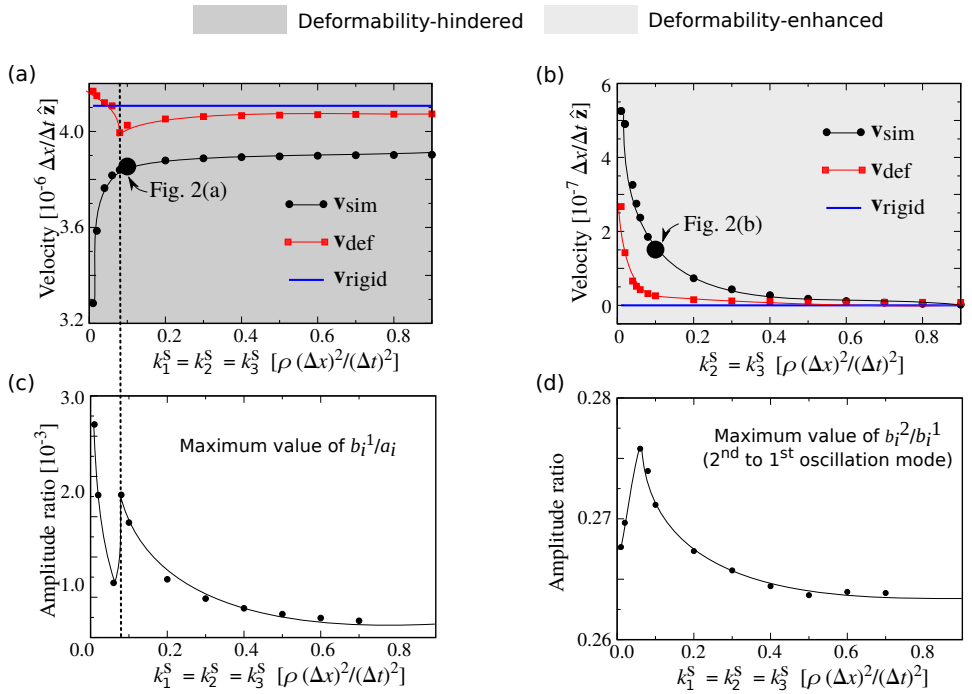

Fig. 4 (Colour online) Comparison of swimmer velocity found from simulations ($\mathbf{v}_{sim}$) and theoretical velocity expressions assuming rigid ($\mathbf{v}_{rigid}$) and deformable ($\mathbf{v}_{def}$) beads, for changing shear moduli k_i^S of the beads. In part (a), the k_i^S values of all the beads are changed together, and the force ratio and the force phase difference respectively are $A/B = 20$ and $\alpha = \pi/2$. In part (b), k_1^S is held constant at $1.0\rho(\Delta x)^2/(\Delta t)^2$ while the k_i^S values for $i = 2,3$ are changed together, and the force ratio and the force phase difference are respectively $A/B = 1$ and $\alpha = 0$. The forcing is symmetric in (b), meaning that in the case of rigid beads ($k_2^S = k_3^S \gtrsim 0.8\rho(\Delta x)^2/(\Delta t)^2$) there is no swimming. Parts (c) and (d) show the (relative) amplitudes of the first and second oscillation modes of the bead surfaces for the simulations presented in part (a). The thin lines (black and red) are meant as guides for sight, while the big black circles mark the simulations presented in Table 1 and Fig. 2.

these the 'deformability-enhanced' and 'deformability-hindered' regions, respectively (here 'deformability' being understood to mean 'the deformability of the i^{th} bead').

To compare the above analytical picture with the simulations, we first extract from the simulations the $b_i^1(t)$ functions for each given combination of the different bead stiffness moduli, and then find the theoretically-expected velocity $\mathbf{v}_{def}$ using Eq. (20). In Fig. 4(a), the velocity of the swimmer in the simulations ($\mathbf{v}_{sim}$, plotted in black circles) increases when the shear moduli of all the beads in the swimmer are gradually increased (meaning when the deformations of the bead surfaces decrease; see Fig. 4(c)). This increase is echoed by the theoretical velocity for swimmers with deformable beads, $\mathbf{v}_{def}$ (red squares), for $k_i^S > 0.08\rho(\Delta x)^2/(\Delta t)^2$. For this k_i^S range, the $\mathbf{v}_{def}$ curve also performs better in comparison to the simulations than the curve obtained using the rigid-bead theory ($\mathbf{v}_{rigid}$, marked as a blue line).

In Fig. 4(b) we present a case of symmetric driving ($A = B$, $\alpha = 0$), which for identical rigid beads results in no net swimming. To obtain swimming behaviour, we let one bead in the swimmer remain rigid, while the shear moduli of the other two beads are varied together ($k_2^S = k_3^S$), thus breaking the symmetry in the setup. Since the velocity is zero for rigid beads, for at least some range of k_i^S we must obtain the deformability-enhanced regime, and this is precisely what the simulations show ($\mathbf{v}_{sim}$) as well as what the deformable bead theory ($\mathbf{v}_{def}$) gives. In this case we find that the theoretical $\mathbf{v}_{def}$ curve shows good qualitative agreement with the simulations ($\mathbf{v}_{sim}$ curve) for $k_2^S = k_3^S > 0.01\rho(\Delta x)^2/(\Delta t)^2$.

In short, in both the simulation sets presented in Fig. 4(a) and (b) as well as in all the other simulations that we have studied, the $\mathbf{v}_{def}$ curve correctly reproduces in the low-deformability limit the velocity trend observed. Due to the small-deformations assumption and the fact that the difference between the deformable bead velocity expression ($\mathbf{v}_{def}$) and the rigid bead one ($\mathbf{v}_{rigid}$) is proportional to the deformations (b_i^1), the $\mathbf{v}_{def}$ curve is quantitatively always a small correction to the $\mathbf{v}_{rigid}$ curve.

For smaller k_i^S values, the theoretical curve can differ qualitatively from the simulation curve. As seen in Fig. 4(c), the b_i^1/a_i ratios for the simulation set of Fig. 4(a) remain small (only the maximum value of this ratio over the three beads for each simulation is displayed). The discrete jump in the $\mathbf{v}_{def}$ curve in Fig. 4(a) at $k_i^S = 0.08\rho(\Delta x)^2/(\Delta t)^2$ is inherited from a similar discrete change in the b_i^1/a_i ratio. Since in our simulations the oscillations of the bead positions are of the same order of magnitude as the mean bead radii, the ratios $b_i^1/|\xi_j(t)|$ remain small too. Moreover, the amplitudes of the higher oscillation modes are successively smaller than that of the first oscillation mode (demonstrated by the maximum ratio of the first two oscillation modes in Fig. 4(d), again for the simulation set of Fig. 4(a)). This replicates the result obtained from the theory, that only the driving frequency mode of bead surface oscillation contributes to the lowest order. These two points imply that the qualitative differences between the theory and the simulations for small k_i^S values must spring from a

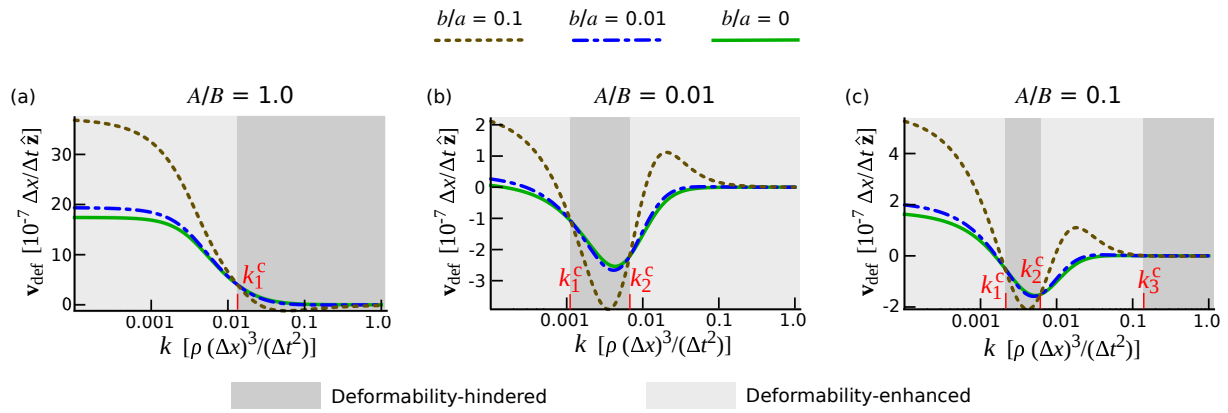

Fig. 5 (Colour online) Velocity vs. effective elastic parameter for swimmers with deformable beads, for different driving force amplitude ratios A/B which result in (a) one, (b) two, and (c) three critical spring constant values k_i^c. The solid green curve is for a swimmer with rigid beads.

breakdown of the assumption of decoupling between the bead deformations and the fluid flow.

6 Active deformations – dynamic state diagram

In the present simulations the surface deformations of the beads cannot be imposed and must be read off from the simulations *a posteriori*. Using our theory, we can overcome this restriction and consider the effect of *active* deformations, which are imposed by the swimmer itself (or by some external control mechanism). For this the theory remains unchanged if these deformations are again considered to be weak enough to justify disregarding the fluid flow induced by them.

For active deformations, we study the velocity dependence on the deformability for the special case of identical beads deforming with equal oscillation amplitudes, *i.e.* with $a_i = a$ and $b_i^1 = b$, for $i = 1,2,3$. The sum of the three m_i's in Eq. (20) can then be redefined as m, and we find that it is the spring constant k which determines whether the swimming is deformability-enhanced ($m > 0$) or deformability-hindered ($m < 0$), independent of the deformation amplitude b of the beads. The condition $m = 0$ (which is equivalent to $\mathrm{d}\mathbf{v}_{\mathrm{def}}/\mathrm{d}b = \mathbf{0}$) yields a cubic equation in terms of k, and we denote the resulting roots as k_i^c ($i = 1,2,3$), which separate the deformability-enhanced and deformability-hindered regions. These critical spring constant values do not depend on the bead oscillations b, since the m_i's in Eq. (20) are independent of b_i^1's. Fig. 5 shows a case in which all three k_i^c values are physically meaningful, *i.e.* real and positive. All the velocity curves, for different b/a ratios, cross each other at the k_i^c values. For explicit expressions for k_i^c, see the *Mathematica* file in the ESI.

In Fig. 6 we present dynamic state diagrams, again for $a_i = a$ and $b_i^1 = b$ (for $i = 1,2,3$), showing the relative extent of the deformability-enhanced and -hindered regions for different driving force amplitude ratios A/B and phase shifts α, for a few values of the spring constant k. In each diagram, all the parameters apart from A/B and α are kept constant. While the precise shapes of the regions depend on the different parameters, the state diagrams exhibit the property that for soft springs (small values of k), the swimmer becomes slower with increasing bead deformability

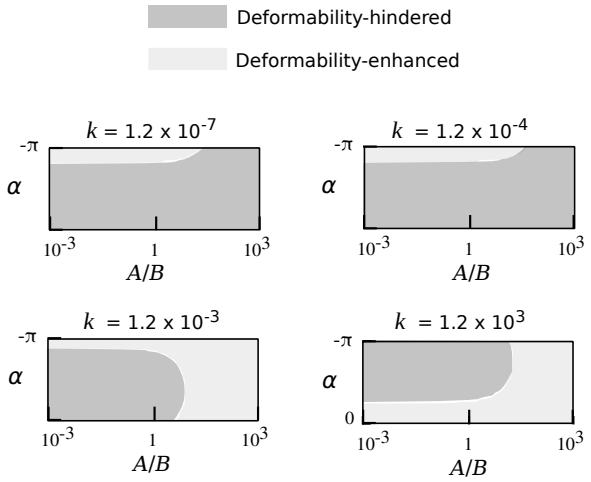

Fig. 6 (Colour online) Dynamic state diagrams for swimmers with deformable beads, showing the dependence of the two marked regimes on the driving force amplitude ratio A/B and driving force phase shift α (see Eq. (2)), for increasing values of the spring constant k (given in units of $\rho(\Delta x)^3/(\Delta t)^2$).

for a majority of the state space. As the springs become stiffer, the swimmer becomes more likely to benefit from an increase in the bead deformabilities. This happens because in the limit of perfectly stiff springs (*i.e.* infinite k), a swimmer with rigid beads cannot swim as it is one contiguous, rigid body, and in this case deformable beads are necessary to gain the requisite degrees of mechanical freedom which may lead to motion.

7 Conclusion

In this work we have studied how deformability in the body of a mechanical microswimmer influences its motion. In particular we have considered the question of whether having a soft body, yielding to the surrounding fluid flow by undergoing shape changes, is beneficial to the motion of a swimmer for which the main mechanism for motility is independent of these shape changes. As our model we have chosen a bead-spring swimmer, where the motion occurs due to the contraction and expansion of the springs in response to driving forces, and where the beads are deformable

and alter their shapes continuously as the swimmer makes its way through the fluid.

We have studied this swimmer through immersed-boundary-lattice-Boltzmann simulations for different stiffness moduli of the beads. These are the first fully-resolved simulations in three dimensions of microswimmers with elasticity both in the body and in the swimming appendage (like flagella). We have found that deformations in the bead surfaces, induced by the pressure of the surrounding fluid, can lead to the swimmer either quickening up or slowing down. Remarkably, the same deformations can produce either effect, depending on the other parameters in the problem.

In order to understand the velocity curves obtained in the simulations, we have derived an analytical expression for the swimming velocity which assumes that the deformations in the beads are small and are *a priori* known functions of time. The calculation shows that only the driving frequency mode of the surface deformations affects the velocity to the lowest order. The final form of the velocity suggests that it can either increase or decrease with the deformations of the beads, but must be a monotonic function of the latter.

Comparing the analytical results to the simulations, we have found that in the limit of small deformations, the theoretical model reproduces correctly the velocity trends, both increase and decrease, with increasing deformability for all the parameter sets studied. It also improves considerably upon the velocity values predicted by a theory which assumes the beads in the swimmer to be rigid. Finally, we have shown that for swimmers with identical deformations in the three beads (such as might be accomplished by actively deforming beads), it is the spring constant which determines whether the deformations promote or hinder the motion.

Our study provides a possible explanation for why some microorganisms such as the euglenid *Eutreptiella gymnastica*[79] undergo a process called *metaboly*, wherein their bodies deform constantly during the swimming motion which is driven mainly by flagella. Both the mechanism and the function of metaboly remain unclear, although there is evidence to suggest that it can be an efficient mode of motility in simple fluids and may become important in granular or complex media.[80] Our results here support this thesis, by showing that in certain parameter ranges passive shape changes can enhance a swimmer's motility. However, these changes of shape can also impede the motility in other ranges of the different swimmer parameters, and it is therefore an important task in the future to identify which of the two effects is dominant in the case of biological swimmers.

Secondly, our results are beneficial for the design of artificial microswimmers, many proposed and experimentally-realised models of which utilise periodically-beating elastic components connected to rigid bodies.[1,25,67,81–83] Our findings underline both qualitatively (in the theory) and quantitatively (in the simulations) how appropriately exploiting body deformability can improve the efficiency of these devices.

It is hoped that a third utility of our work will be in its analytical treatment of what is in general a very difficult problem, namely the deformations and consequent effect on swimming of a non-rigid membrane through a fluid, and that in the future this can be extended to an analytical model where these deformations are calculated *a priori*, at least in the small deformation limit.

8 Acknowledgements

A.-S. S. and J. P. thank the funding of the European Research Council (ERC) and of the Deutsche Forschungsgemeinschaft (DFG) through the Cluster of Excellence: Engineering of Advanced Materials. J. H. acknowledges support by NWO/STW (Vidi grant 10787) and L. M. thanks the DAAD for a RISE scholarship. T. K. thanks the University of Edinburgh for the award of a Chancellor's Fellowship.

9 Appendix A1

Here we present the different contributions to the deformation energy of each bead, which arises from shearing and local area dilation, bending, and global volume change (but not from global area change, which is freely allowed).[84] Note that the following are the expressions for the different energy contributions as used in the numerical simulations. In our analytical theory (section 4) we do not use these expressions and instead base the theory on the instantaneous effective hydrodynamic radii $r_i(t)$ of the beads as they undergo the different kinds of deformation here listed.

The strain energy W_i^{S} of the i^{th} bead, which includes both shearing and local area dilation contributions, is given (in accordance with the Skalak model[85]) by

$$W_i^{\mathrm{S}} = \oint \left[\frac{k_i^{\mathrm{S}}}{12} \left(I_{i1}^2 + 2I_{i1} - 2I_{i2} \right) + \frac{k_i^{\alpha}}{12} I_{i2}^2 \right] \mathrm{d}A_i, \tag{21}$$

where k_i^{S} and k_i^{α} denote the shear modulus and the area dilation modulus, respectively, I_{i1} and I_{i2} are strain invariants which depend only on the local principal in-plane stretch ratios,[72] and $\mathrm{d}A_i$ denotes an area element on the surface of the bead.

The bending energy W_i^{B} is a simplified form of the Helfrich function[86] and is given by

$$W_i^{\mathrm{B}} = \frac{\sqrt{3} k_i^{\mathrm{B}}}{2} \sum_{<j,k>} \left(\theta_{ijk} - \theta_{ijk}^{\mathrm{eq}} \right)^2, \tag{22}$$

where k_i^{B} is the bead bending modulus, θ_{ijk} is the normal-to-normal angle between two triangular mesh elements (denoted by j and k) on the surface with a common edge, and $\theta_{ijk}^{\mathrm{eq}}$ is its equilibrium value which is determined by the initial spherical shape of the beads.[72] The sum is taken over all the neighbouring mesh element pairs j and k.

Finally, the volume change energy W_i^{V} is given simply in terms of the deviation from the initial volume $V_i^{(0)}$ as

$$W_i^{\mathrm{V}} = \frac{k_i^{\mathrm{V}}}{2} \frac{\left(V_i - V_i^{(0)} \right)^2}{V_i^{(0)}} \tag{23}$$

where k_i^{V} denotes the bead volume modulus and V_i the instantaneous bead volume.[72]

10 Appendix A2

Here we present the expression for the velocity $\mathbf{v}_{\text{rigid}}$ of a swimmer with three rigid beads of constant effective hydrodynamic radii r_i $(i = 1,2,3)$ in terms of the other parameters defined, following the calculation in Pickl *et al.*[74] For the driving force parameters specified by Eq. (2) and with k and η denoting the spring constant and the dynamic viscosity of the fluid, respectively, the velocity $\mathbf{v}_{\text{rigid}}$ is

$$\mathbf{v}_{\text{rigid}} = \frac{N}{D}\hat{\mathbf{z}}, \tag{24}$$

where

$$\begin{aligned} N = 21 r_1 r_2 r_3 \omega \Big\{ & 6\left(A^2 - B^2\right) r_1 r_3 k \pi \eta \omega \\ & + AB\left[\left(r_1 + r_2 + r_3\right) k^2 + 36 r_1 r_2 r_3 \pi^2 \eta^2 \omega^2\right] \sin\alpha \\ & + 6AB\left(r_1 - r_3\right) r_2 k \pi \eta \omega \cos\alpha \Big\}, \end{aligned} \tag{25}$$

and

$$\begin{aligned} D = 8\left(r_1 + r_2 + r_3\right) l^2 \Big\{ & \left(r_1^2 + r_2^2 + r_3^2 + 2r_1 r_2 + 2r_2 r_3 + 2r_3 r_1\right) k^4 \\ & + 36\left[r_2^2\left(r_1^2 + r_3^2\right) + 2r_1 r_2 r_3\left(r_1 + r_3\right) \right. \\ & \left. + 4 r_1^2 r_3^2\right] k^2 \pi^2 \eta^2 \omega^2 \\ & + 1296 r_1^2 r_2^2 r_3^2 \pi^4 \eta^4 \omega^4 \Big\}. \end{aligned} \tag{26}$$

References

1 R. Dreyfus, J. Baudry, M. L. Roper, M. Fermigier, H. A. Stone and J. Bibette, *Nature*, 2005, **437**, 862.

2 K. Ishiyama, M. Sendoh, A. Yamazaki and K. I. Arai, *Sensor Actuat. A-Phys.*, 2001, **91**, 141.

3 J. J. Benkoski, J. L. Breidenich, O. M. Uy, A. T. Hayes, R. M. Deacon, H. B. Land, J. M. Spicer, P. Y. Keng and J. Pyun, *J. Mater. Chem.*, 2011, **21**, 7314.

4 Y.-H. Li, S.-T. Sheu, J.-M. Pai and C.-Y. Chen, *J. Appl. Phys.*, 2012, **111**, 07A924.

5 J. L. Breidenich, M. C. Wei, G. V. Clatterbaugh, J. J. Benkoski, P. Y. Keng and J. Pyun, *Soft Matter*, 2012, **8**, 5334.

6 L. Baraban, D. Makarov, R. Streubel, I. Mönch, D. Grimm, S. Sanchez and O. G. Schmidt, *ACS Nano*, 2012, **6**, 3383.

7 L. Baraban, M. Tasinkevych, M. N. Popescu, S. Sanchez, S. Dietrich and O. G. Schmidt, *Soft Matter*, 2012, **8**, 48.

8 N. C. Keim, M. Garcia and P. E. Arratia, *Phys. Fluids*, 2012, **24**, 081703.

9 I. Theurkauff, C. Cottin-Bizonne, J. Palacci, C. Ybert and L. Bocquet, *Phys. Rev. Lett.*, 2012, **108**, 268303.

10 T. Sanchez, D. Welch, D. Nicastro and Z. Dogic, *Science*, 2011, **333**, 456.

11 Q. Liao, G. Subramanian, M. P. DeLisa, D. L. Koch and M. Wu, *Phys. Fluids*, 2007, **19**, 061701.

12 M. Leoni, J. Kotar, B. Bassetti, P. Cicuta and M. C. Lagomarsino, *Soft Matter*, 2009, **5**, 472.

13 C. M. Pooley, G. P. Alexander and J. M. Yeomans, *Phys. Rev. Lett.*, 2007, **99**, 228103.

14 J. Elgeti and G. Gompper, *Proc. Natl. Acad. Sci. USA*, 2013, **110**, 4470.

15 A. Zöttl and H. Stark, *Phys. Rev. Lett.*, 2012, **108**, 218104.

16 K. Pickl, J. Götz, K. Iglberger, J. Pande, K. Mecke, A.-S. Smith and U. Rüde, *J. of Comp. Sci.*, 2012, **3**, 374.

17 J. W. Swan, J. F. Brady, R. S. Moore and C. 174, *Phys. Fluids*, 2011, **23**, 071901.

18 S. Günther and K. Kruse, *EuroPhys. Lett.*, 2008, **84**, 68002.

19 L. E. Becker, S. A. Koehler and H. A. Stone, *J. Fluid Mech.*, 2003, **490**, 15.

20 R. Ledesma-Aguilar, H. Löwen and J. M. Yeomans, *Eur. Phys. J. E*, 2012, **35**, 70.

21 J. E. Avron, O. Kenneth and D. H. Oaknin, *New J. Phys.*, 2005, **7**, 234.

22 B. M. Friedrich and F. Jülicher, *Phys. Rev. Lett.*, 2012, **109**, 138102.

23 S. Fürthauer and S. Ramaswamy, *Phys. Rev. Lett.*, 2013, **111**, 238102.

24 M. Leoni and T. B. Liverpool, *Phys. Rev. Lett.*, 2010, **105**, 238102.

25 E. M. Purcell, *Am. J. Phys.*, 1977, **45**, 3.

26 C. Chapman-Andresen, *Carlsberg Res. Commun.*, 1976, **41**, 191.

27 W. R. DiLuzio, L. Turner, M. Mayer, P. Garstecki, D. B. Weibel, H. C. Berg and G. M. Whitesides, *Nature*, 2005, **435**, 1271.

28 M. Kreutz, T. Stoeck and W. Foissner, *J. Eukaryot. Microbiol.*, 2012, **59**, 548.

29 H. S. Fisher, L. Giomi, H. E. Hoekstra and L. Mahadevan, *Proc. R. Soc. B*, 2014, **281**, 20140296.

30 N. Ueki, T. Ide, S. Mochiji, Y. Kobayashi, R. Tokutsu, N. Ohnishi, K. Yamaguchi, S. Shigenobu, K. Tanaka, J. Minagawa, T. Hisabori, M. Hirono and K. Wakabayashi, *Proc. Natl. Acad. Sci. USA*, 2016, **113**, 5299.

31 R. Golestanian, T. B. Liverpool and A. Armand, *Phys. Rev. Lett.*, 2005, **94**, 220801.

32 J. R. Howse, R. A. L. Jones, A. J. Ryan, T. Gough, R. Vafabakhsh and R. Golestanian, *Phys. Rev. Lett.*, 2007, **99**, 048102.

33 U. M. Córdova-Figueroa and J. F. Brady, *Phys. Rev. Lett.*, 2008, **100**, 158303.

34 R. M. Erb, N. J. Jenness, R. L. Clark and B. B. Yellen, *Adv. Mater.*, 2009, **21**, 4825.

35 S. J. Ebbens and J. R. Howse, *Soft Matter*, 2010, **6**, 726.

36 I. Buttinoni, G. Volpe, F. Kümmel, G. Volpe and C. Bechinger, *J. Phys.: Cond. Mat.*, 2012, **24**, 284129.

37 P. K. Ghosh, V. R. Misko, F. Marchesoni and F. Nori, *Phys. Rev. Lett.*, 2013, **110**, 268301.

38 M. T. Downton and H. Stark, *Eur. Phys. Lett.*, 2009, **85**, 44002.

39 R. Ledesma-Aguilar and J. M. Yeomans, *Phys. Rev. Lett.*, 2013, **111**, 138101.

40 M. A. Dias and T. R. Powers, *Phys. Fluids*, 2013, **25**, 101901.
41 T. K. Chaudhury, *J. Fluid Mech.*, 1979, **95**, 189.
42 H. C. Fu, V. B. Shenoy and T. R. Powers, *EPL (Europhys. Lett.)*, 2010, **91**, 24002.
43 J. Teran, L. Fauci and M. Shelley, *Phys. Rev. Lett.*, 2010, **104**, 038101.
44 S. E. Spagnolie, B. Liu and T. R. Powers, *Phys. Rev. Lett.*, 2013, **111**, 068101.
45 D. A. Gagnon, X. N. Shen and P. E. Arratia, *EPL (Europhys. Lett.)*, 2013, **104**, 14004.
46 B. Thomases and R. D. Guy, *Phys. Rev. Lett.*, 2014, **113**, 098102.
47 E. E. Riley and E. Lauga, *J. Theor. Biol.*, 2015, **382**, 345.
48 G. Li and A. M. Ardekani, *J. Fluid Mech.*, 2015, **784**, R4.
49 J. K. Wróbel, S. Lynch, A. Barrett, L. Fauci and R. Cortez, *J. Fluid Mech.*, 2016, **792**, 775.
50 R. Kusters, T. van der Heijden, B. Kaoui, J. Harting and C. Storm, *Phys. Rev. E*, 2014, **90**, 033006.
51 J. Pande and A.-S. Smith, *Soft Matter*, 2015, **11**, 2364.
52 N. Küchler, H. Löwen and A. M. Menzel, *Phys. Rev. E*, 2016, **93**, 022610.
53 A. Farutin, S. Rafaï, D. K. Dysthe, A. Duperray, P. Peyla and M. Chaouqi, *Phys. Rev. Lett.*, 2013, **111**, 228102.
54 H. Wu, M. Thiébaud, W.-F. Hu, A. Farutin, S. Rafaï, M.-C. Lai, P. Peyla and C. Misbah, *Phys. Rev. E*, 2015, **92**, 050701(R).
55 J. G. Mitchell, *Am. Nat.*, 2002, **160**, 727.
56 T. Ohta and T. Ohkuma, *Phys. Rev. Lett.*, 2009, **102**, 154101.
57 T. Ohta, T. Ohkuma and K. Shitara, *Phys. Rev. E*, 2009, **80**, 056203.
58 T. Hiraiwa, M. Y. Matsuo, T. Ohkuma, T. Ohta and M. Sano, *Europhys. Lett.*, 2010, **91**, 20001.
59 T. Ohkuma and T. Ohta, *Chaos*, 2010, **20**, 023101.
60 M. Tarama and T. Ohta, *Eur. Phys. J. B*, 2011, **83**, 391.
61 K. Shitara, T. Hiraiwa and T. Ohta, *Phys. Rev. E*, 2011, **83**, 066208.
62 T. Hiraiwa, K. Shitara and T. Ohta, *Soft Matter*, 2011, **7**, 3083.
63 Y. Itino, T. Ohkuma and T. Ohta, *J. Phys. Soc. Japan*, 2011, **80**, 033001.
64 Y. Itino and T. Ohta, *J. Phys. Soc. Japan*, 2012, **81**, 104007.
65 A. M. Menzel and T. Ohta, *Europhys. Lett.*, 2012, **99**, 58001.
66 M. Tarama, A. M. Menzel, B. ten Hagen, R. Wittkowski, T. Ohta and H. Löwen, *J. Chem. Phys.*, 2013, **139**, 104906.
67 A. Najafi and R. Golestanian, *Phys. Rev. E*, 2004, **69**, 062901.
68 F. Jansen and J. Harting, *Phys. Rev. E*, 2011, **83**, 046707.
69 T. Krüger, S. Frijters, F. Günther, B. Kaoui and J. Harting, *Eur. Phys. J. Spec. Top.*, 2013, **222**, 177.
70 T. Krüger, H. Kusumaatmaja, A. Kuzmin, O. Shardt, G. Silva and E. M. Viggen, *The Lattice Boltzmann Method*, Springer, 2017.
71 C. S. Peskin, *Acta Numer.*, 2002, **11**, 479.
72 T. Krüger, F. Varnik and D. Raabe, *Comput. Math. Appl.*, 2011, **61**, 3485.
73 F. Perrin, *J. Phys. Radium*, 1934, **5**, 497.
74 K. Pickl, J. Pande, H. Köstler, U. Rüde and A.-S. Smith, *J. Phys.: Condens. Matter*, 2017, **29**, 124001.
75 M. Doi and S. F. Edwards, *The Theory of Polymer Dynamics*, Oxford University Press, U.S.A., 1988.
76 J. Happel and H. Brenner, *Low Reynolds Number Hydrodynamics*, Prentice-Hall Inc., 1965.
77 C. W. Oseen, *Neuere Methoden und Ergebnisse in der Hydrodynamik*, Leipzig: Akademische Verlagsgesellschaft, 1927.
78 B. U. Felderhof, *Phys. Fluids*, 2006, **18**, 063101.
79 J. Throndsen, *Norwegian J. Botany*, 1969, **16**, 161.
80 M. Arroyo, L. Heltai, D. Millán and A. DeSimone, *Proc. Natl. Acad. Sci. USA*, 2012, **109**, 17874.
81 G. Taylor, *Proc. R. Soc. Lond. A*, 1951, **209**, 447.
82 J. Elgeti, U. B. Kaupp and G. Gompper, *Biophys. J.*, 2010, **99**, 1018.
83 B. J. Williams, S. V. Anand, J. Rajagopalan and M. T. A. Saif, *Nat. Commun.*, 2014, **5**, 3081.
84 T. Krüger, M. Gross, D. Raabe and F. Varnik, *Soft Matter*, 2013, **9**, 9008.
85 R. Skalak, A. Tozeren, R. P. Zarda and S. Chien, *Biophys. J.*, 1973, **13**, 245.
86 W. Helfrich, *Z. Naturforsch. C*, 1973, **28**, 693.